European Journal of Pharmaceutical Sciences 179 (2022) 106309

Contents lists available at ScienceDirect

European Journal of Pharmaceutical Sciences

journal homepage: www.elsevier.com/locate/ejps

# Assessing the contribution of UGT isoforms on raltegravir drug disposition through PBPK modeling

Fernanda-de-Lima Moreira [a], Maria-Martha-de-Barros Tarozzo [b], Glauco-Henrique-Balthazar Nardotto [b], José-Carlos-Saraiva Gonçalves [a], Stephan Schmidt [c], Natália-Valadares de-Moraes [c,*]

[a] Faculdade de Farmácia, Universidade Federal do Rio de Janeiro, Rio de Janeiro, RJ, Brazil
[b] Departamento de Análises Clínicas, Toxicológicas e Bromatológicas, Faculdade de Ciências Farmacêuticas de Ribeirão Preto, Universidade de São Paulo, Ribeirão Preto, SP, Brazil
[c] Center for Pharmacometrics and Systems Pharmacology, Department of Pharmaceutics, College of Pharmacy, University of Florida, 6550 Sanger Road, Lake Nona, Orlando, FL, USA

ARTICLE INFO

*Keywords:*
UDP-glucuronosyltransferase
UGT1A1
UGT1A3
HIV
PBPK modeling and simulation

ABSTRACT

This work aimed to develop a physiologically based pharmacokinetic (PBPK) model for raltegravir accounting for UDP-glucuronosyltransferase (UGT) metabolism to assess the effect of UGT gene polymorphisms. Raltegravir elimination was evaluated using $K_m$ and $V_{max}$ values from human recombinant systems and UGT tissue scalar considering liver, kidney, and intestine. The predicted/observed ratios for raltegravir PK parameters were within a 2-fold error range in UGT1A1 poor and normal metabolizers, except in Asian UGT1A1 poor metabolizers. This PBPK modeling approach suggests that UGT1A3 is the main contributor to raltegravir's metabolism. UGT1A3 and UGT1A1 gene polymorphisms might have an additive effect on raltegravir's drug disposition and response. The final model accounting for hepatic, renal, and intestinal UGT metabolism, biliary clearance, and renal excretion improved model predictions compared with the previously published models. This PBPK model with the quantitative characterization of raltegravir elimination pathways can support dose adjustments in different clinical scenarios.

## 1. Introduction

Model-informed precision dosing requires the quantitative assessment of elimination pathways to predict drug disposition accurately. Physiologically based pharmacokinetic (PBPK) models have gained prominence and regulatory acceptance for evaluating drug-drug interactions, pharmacogenetics, and special populations in recent years. These PBPK applications hinge on the availability of high-quality enzyme and transporter data (European Medicines Agency, 2015; Jones and Rowland-Yeo, 2013). For example, a PBPK model to support phenotype-guided dose adjustment requires quantitative characterization of elimination pathways, including enzyme kinetic parameters, transport-metabolism interplay when appropriate, and well-designed clinical data to verify model predictions (Peters et al., 2019). However, abundance and functionality assessments for non-CYP enzymes and drug transporters are current knowledge gaps that hinder the even broader application of PBPK modeling and simulation (Ladumor et al., 2019).

UDP-glucuronosyltransferase (UGT) isoforms catalyze glucuronidation reactions of many endogenous substrates and drugs such as raltegravir, irinotecan, and telmisartan. Genetic polymorphisms in the alleles encoding UGT isoforms result in reduced expression levels or lower *in vitro/in vivo* activity Kasteel et al., 2020). Consequently, polymorphic variants associated with low enzyme UGT activity result in increased drug exposure and potentially drug-induced toxicity. Raltegravir is an HIV-integrase inhibitor eliminated primarily by UGT enzymes. *In vitro* studies using recombinant UGT showed that raltegravir metabolism is mediated mainly by UGT1A1, UGT1A9, and UGT1A3 (Kassahun et al., 2007). High inter-patient variability in raltegravir pharmacokinetics has been reported (Cattaneo et al., 2012). UGT1A1*28 carriers showed higher raltegravir plasma concentrations and lower metabolic ratio when compared with homozygous

* Corresponding author.
*E-mail address:* nataliademoraes@ufl.edu (N.-V. de-Moraes).

https://doi.org/10.1016/j.ejps.2022.106309
Received 24 June 2022; Received in revised form 13 September 2022; Accepted 16 October 2022
Available online 17 October 2022

UGT1A1*1/*1 (Belkhir et al., 2018). Although other UGT isoforms play a role in raltegravir elimination, their contribution to pharmacokinetics or clinical outcomes is unknown.

Raltegravir is administered orally twice daily with an usual dose of 400 mg. It reaches a steady-state maximum plasma concentration ($C_{max}$) of 1,000 to 3,000 ng/mL in the fasted state (Andrews et al., 2010; Brainard et al., 2011a; Hanley et al. 2009; Iwamoto et al., 2008a; Krishna et al., 2018; Neely et al., 2010; Rizk et al., 2012; Taburet et al., 2015; Weiner et al., 2014). It is well-tolerated even at higher doses (800 mg twice a day administered for 10 days) (Iwamoto et al., 2008a). The excretion of unchanged raltegravir in feces accounts for 51 (± 10) % of the dose. The high concentrations of glucuronide in the bile and the high amount of unchanged drug recovered in feces support the participation of gastrointestinal glucuronidase in raltegravir metabolism (Kassahun et al., 2007). In urine, 32 (± 9) % of the dose was recovered as raltegravir and raltegravir-glucuronide, each accounting for 9% and 23%, respectively (Kassahun et al., 2007). Secondary peaks are often observed in pharmacokinetic studies (Blonk et al., 2015; Rizk et al., 2012; Taburet et al., 2015; Watts et al., 2014), and the reasonable explanations are the delayed absorption or the entero-hepatic recycling. *In vitro* studies with liver, intestine, and kidney subcellular fractions indicate the participation of different tissues in raltegravir glucuronidation (Liu et al., 2019). Our goal was to develop a PBPK model accounting for UGT 1A1, 1A3, 1A7, 1A8, and 1A9-mediated metabolism isoenzymes on raltegravir disposition (Liu et al., 2019). Simulations were performed with the final PBPK model to show the impact of UGT1A1 and UGT1A3 genetic polymorphisms on raltegravir plasma concentration-time profiles.

## 2. Methods

### 2.1. PBPK model strategy

PBPK modeling and simulation were performed using Simcyp v. 20 (Certara, Princeton, NJ). The drug file containing compound properties for raltegravir (SV-raltegravir) in Simcyp was used as a base model for further development, refinement, and verification processes (Table 1). A full-body PBPK model was developed for raltegravir in healthy volunteers for 400 mg oral administration single or twice-daily doses. The model was verified by comparing model-based simulations with observed *in vivo* concentration-time profiles obtained from published clinical studies. Raltegravir concentration-time profiles were extracted using a web-based data extraction tool (https://automeris.io/WebPlotDigitizer/). The enzyme kinetics data for UGT1A1, 1A3, 1A9, 1A7, and 1A8, biliary clearance, and entero-hepatic circulation were incorporated into the raltegravir PBPK model. Human physiological parameters were available in the virtual population of healthy volunteers (Sim-Healthy Volunteers) implemented in Simcyp. Fig. 1 describes the PBPK model building and verification workflow to evaluate raltegravir disposition. The PBPK model developed here was compared with three previous published raltegravir PBPK models (Table 1) (Liu et al., 2020; Moss et al., 2013; Sychterz et al., 2021).

Model predictions were evaluated using a single oral dose (400 mg) or twice-daily doses (400 mg BID) of raltegravir. The model was verified using clinical data from healthy volunteers for the single-dose regimen (Blonk et al., 2012; Iwamoto et al., 2008a; Iwamoto et al., 2008b; Wang et al., 2011; Wenning et al., 2009a). Raltegravir steady-state concentrations were verified with observed PK data in healthy and HIV-infected adult subjects (Andrews et al., 2010; Brainard et al., 2011a; Hanley et al., 2009; Iwamoto et al., 2008a; Krishna et al., 2018; Neely et al., 2010; Rizk et al., 2012; Taburet et al., 2015; Weiner et al., 2014). Simulated concentration-time profiles for single or multiple doses were verified using clinical data reported from UGT1A1 polymorphisms studies (Belkhir et al., 2018; Wenning et al., 2009b; Yagura et al., 2015). All simulations were carried out in 10 virtual trials with 10 subjects each, in the fasted state and using the same dosing regimen, the

**Table 1**
Summary of input data for raltegravir physiologically based pharmacokinetic models of the present work and the published articles.

| Parameters | Liu et al. (2020) | Sychterz et al. (2021) | Moss et al. (2013) | Present work |
|---|---|---|---|---|
| Physical chemistry | | | | |
| Molecular weight (g/mol) | 444.42 | 444.42 | 445.16 | 444.42 |
| log P | 0.58 | 1.07[a] | 0.58 | 1.07[a] |
| pka (monoprotic acid) | 6.67 | 6.7[a] | 6.67 | 6.7[a] |
| fraction unbound | 0.17 | 0.17[a] | 0.17 | 0.17[a] |
| B/P | | 0.62[a] | 0.6 | 0.62[a] |
| Absorption | | | | |
| intestinal permeability (transcellular) [$10^{-5}$ cm/min] | 1.71[b] | | | |
| Model | | first-order absorption[a] | | ADAM |
| fa | 1 | | | |
| ka (1/h) | 0.4 | | | |
| lag time (h) | 0.3 | | | |
| Caco-2 pH 6.5:7.4 ($10^{-6}$ cm/s) | | | | 9.2[d] |
| Caco-2 pH 7.4:7.4 ($10^{-6}$ cm/s) | | | 6.6[d] | |
| Distribution | Rogers and Rowland | Poulin and Theil; full PBPK model | Poulin and Theil; full PBPK model | Poulin and Theil; full PBPK model |
| Kp scalar | | 1 | | 1 |
| Vss/F (L/kg) | | 0.34 | | 0.34 |
| Elimination | | | | |
| hepatic $Cl_{int}$ uL/min/$10^6$ hepatocytes | | | 12.4[e] | |
| $K_m$ UGT1A1 [μM] | 99[c] | | | |
| $V_{max}$ UGT1A1 [nmol/min/mg] | 2.74[b] | | | |
| $K_m$ UGT1A9 [μM] | 296[c] | | | |
| $V_{max}$ UGT1A9 [nmol/min/mh] | 1.63[b] | | | |
| UGT1A1 $Cl_{int}$ [μL/min/pmol] | | 1.48[a] | | |
| $fu_{inc}$ | | 1[a] | | |
| ISEF | | 1[a] | | |
| $K_m$ UGT1A1 [μM] | | | | 260[g] |
| $V_{max}$ UGT1A1 [pmol/min/mg] | | | | 334[g] |
| $fu_{inc}$ UGT1A1 | | | | 1 |
| $K_m$ UGT1A3 [μM | | | | 41[g] |
| $V_{max}$ UGT1A3 [pmol/min/mg] | | | | 30[g] |
| $fu_{inc}$ UGT1A3 | | | | 1 |
| $K_m$ UGT1A9 [μM] | | | | 193[g] |
| $V_{max}$ UGT1A9 [pmol/min/mg] | | | | 459[g] |
| $fu_{inc}$ UGT1A9 | | | | 1 |
| Km UGT1A7 [μM] | | | | 452[g] |
| $V_{max}$ UGT1A7 [pmol/min/mg] | | | | 23[g] |
| $fu_{inc}$ UGT1A7 | | | | 1 |
| Km UGT1A8 [μM] | | | | 386[g] |
| $V_{max}$ UGT1A8 [pmol/min/mg] | | | | 39[g] |
| $fu_{inc}$ UGT1A8 | | | | 1 |
| $Cl_{int}$ biliary [μL/min$10^6$] (CV) | | | | 12 (30)[h] |
| $CL_R$ (L/h) | | 3.3[a] | 3.6[f] | 3.3[i] |

[a] default compound file parameters provided in Simcyp software
[b] fitted
[c] Kassahun et al. (2007)
[d] Moss et al. (2012)
[e] fitted using Wang et al. (2011)
[f] Iwamoto et al. (2008a)

[g] Liu et al. (2019)
[h] fitted to clinical data
[i] Neely et al. (2010)

proportion of females, and age range described in each clinical study. For multiple-dose studies, the simulations were conducted for 15 days (total duration of 372 h), and the concentration-time profile in the last dose administration interval (360 to 372 h) was assessed. The PBPK model was evaluated by visually comparing observed plasma concentration-time profiles with the predicted plasma concentrations in healthy virtual volunteers. The ratios of predicted/observed pharmacokinetic parameters - area under the curve plasma concentration versus time (AUC) extrapolated to infinity ($AUC_{0-\infty}$), time to reach $C_{max}$ ($T_{max}$), $C_{max,}$ and total clearance (CL/F) - were calculated, and the number of ratios within a 2-fold error range ($0.5 \leq$ ratio $\leq 2$) was recorded.

### 2.2. Development and verification of a PBPK model of raltegravir in healthy volunteers - single oral dose

Since the Simcyp V20 default raltegravir file does not account for all UGT isoenzymes, glucuronidation by different tissues, biliary clearance, and entero-hepatic recycling, it does not appropriately capture the clinical concentration-time profiles (Figs. S1 and S2). Consequently, model setup and parameterization were critically reviewed and updated as follows. The default physicochemical parameters of raltegravir (molecular weight, log P, pKa) were maintained (Table 1). In the absence of intravenous pharmacokinetic data, drug parameters related to the oral absorption model were evaluated. The Advanced Dissolution, Absorption, and Metabolism (ADAM) model using either the mechanistic permeability ($MechP_{eff}$) model or *in vitro* permeability data in Caco-2 cells with active and passive transport at pH 7.4:7.4 ($6.6 \times 10^{-6}$ cm/s) or pH 6.5:7.4 ($9.2 \times 10^{-6}$ cm/s) (Moss et al., 2011) was evaluated for the prediction of the human jejunum effective permeability ($10^{-4}$ cm/s) ($P_{eff,man}$). The absorption profile predictions based on the $MechP_{eff}$ model based on physicochemical inputs and Caco-2 pH 6.5:7.4 $9.2 \times 10^{-6}$ cm/s resulted in similar absorption profiles. Both were superior to the first-order absorption model used in the default model. Based on Caco-2 cells, $P_{eff,man}$ value of $2.09 \times 10^{-4}$ cm/s. The lag time of 0.3 h from the absorption default model was kept in the model.

Following the optimization of the absorption process, the predictions of the volume of distribution at steady state ($V_{ss}$) were evaluated. Tissue-to-plasma partition coefficients (Kp) were estimated using Poulin and Theil method (Method 1) in a full PBPK perfusion-limited distribution model. The predicted $V_{ss}$ was 0.34 l/kg.

Systemic clearance of raltegravir was mediated by UGT isoenzymes, biliary clearance, and renal clearance (Table 1). Based on the literature, the renal clearance was set to 3.3 L/h (Neely et al., 2010). *In vitro* data of raltegravir glucuronidation were obtained from Liu et al. (2019). First, the systemic clearance was predicted using the Michaelis Menten constant ($K_m$) and the maximum rate of metabolism ($V_{max}$) or the $Cl_{int}$ values obtained from human liver, intestine, and kidney microsomes. Nevertheless, the predicted systemic clearance was approximately 4-fold lower than the observed one (Fig. S3). Since the simulation based on *in vitro* data from human microsomes did not adequately predict raltegravir clearance, the next step in the model building was the evaluation of the *in vitro* metabolism from recombinant UGT isoenzymes (Liu et al., 2019). $K_m$ and $V_{max}$ or $Cl_{int}$ values from recombinant UGT1A1, UGT1A3, UGT1A7, UGT1A8, and UGT1A9 isoforms were incorporated into the elimination model. As the results obtained using $K_m$ and $V_{max}$ values were similar to that using $Cl_{int}$ values, the first one was selected. The correction of the contribution of each UGT isoenzyme in each tissue (liver, kidney, or intestine) was considered using the rhUGT tissue scalar approach. The rhUGT tissue scalars (Table 2) were calculated for each drug-metabolizing isoenzyme by the equation:

$$\frac{rhUGT}{tissue\ scalar} = \frac{V_{max}\ (HLM\ or\ HIM\ or\ HKM)}{V_{max} rhUGT}$$

HLM, HIM, and HKM are human microsomes obtained from the liver,

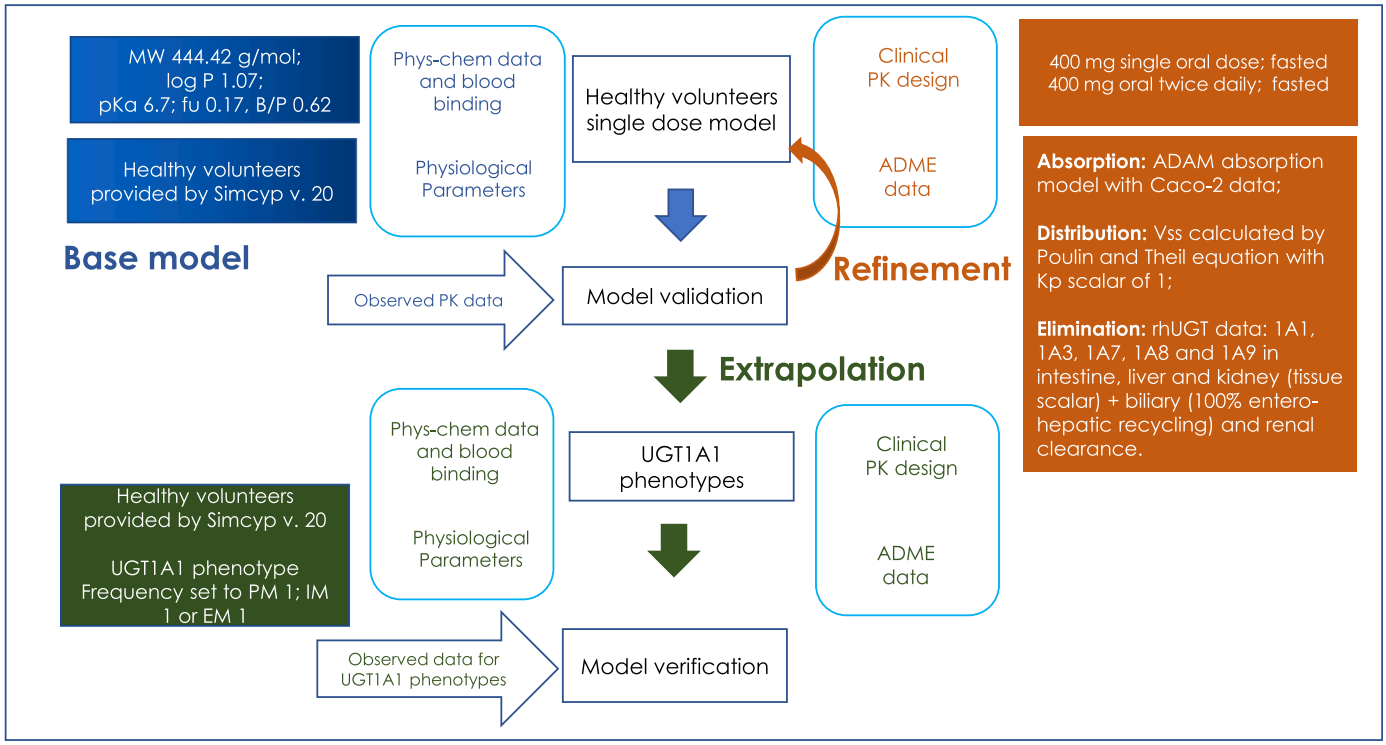


**Fig. 1.** PBPK model building and verification workflow for raltegravir disposition in healthy volunteers and the effect of UGT1A1 gene polymorphisms. Abbreviations: MW: Molecular weight, fu: fraction unbound, B/P: blood to plasma ratio; PM: poor metabolizer IM: intermediate metabolizer, NM: normal metabolizer; UGT: UDP-glucuronosyltransferase.

**Table 2**
Tissue scalar factor for UDP-glucuronosyltransferases (UGT) isoenzymes.

| UGT | tissue scalar liver | kidney | intestine |
|---|---|---|---|
| 1A1 | 5.20 | 6.98 | 0.98 |
| 1A3 | 57.9 | 0 | 10.87 |
| 1A7 | 0[a] | 101.39 | 14.17 |
| 1A8 | 0 | 59.79 | 8.36 |
| 1A9 | 3.78 | 5.08 | 0.71 |

[a] isoform not expressed in the tissue.

intestine, and kidney. $V_{max}$ is the maximum rate of a metabolic pathway, and rhUGT is the human recombinant UGT isoform. Finally, the intrinsic biliary clearance was fitted to oral PK data (Andrews et al., 2010; Brainard et al., 2011a; Hanley et al., 2009; Iwamoto et al., 2008a; Krishna et al., 2018; Neely et al., 2010; Rizk et al., 2012; Taburet et al., 2015; Weiner et al., 2014).

### 2.3. PBPK model verification and refinement

#### 2.3.1. Raltegravir administered in twice-daily oral doses

After successful PBPK simulations for raltegravir as single oral dosing, simulations were performed to predict pharmacokinetic profiles and parameters after twice-daily oral doses of 400 mg raltegravir in the fasted state. In addition, enterohepatic recirculation (EHR) may be a critical process for glucuronide metabolites. Raltegravir glucuronides are eliminated through biliary excretion (Reddy et al., 2021). Due to the lack of *in vitro* data to support the addition of EHR to raltegravir model, a non-mechanistic approach was applied. After a sensitivity analysis, the biliary clearance was optimized to 12 μL/min/$10^{-6}$. The proportion of drug cleared by the biliary route that is available for reabsorption was set as 100% in the final PBPK model to account for the extent of conjugated metabolite reconverted to the parent drug in the gut lumen. Later, the biliary clearance value and the reabsorption percentage were incorporated into the single oral dose PBPK model.

### 2.4. Simulation of UGT1A1 polymorphism impact on raltegravir pharmacokinetics

The classification for UGT1A1 genotype-predicted phenotype was in line with the Clinical Pharmacogenetics Implementation Consortium and defined as follows: normal metabolizers (*1/*1; *1/*36; *36/*36), intermediate metabolizers (*1/*28; *1/*6), and poor metabolizers (*28/*28; *6/*28; *6/*6) (Gammal et al., 2016). After verification, PBPK simulations were performed to assess the effect of UGT1A1 polymorphism on raltegravir pharmacokinetics. The frequency of UGT1A1 poor, intermediate or normal metabolizer in Simcyp was set as 1 (100%) for simulations of each phenotype. Predicted raltegravir data in UGT1A1 poor, intermediate, and normal metabolizers were compared to reported clinical data on UGT1A1 genotypes (Belkhir et al., 2018; Wenning et al., 2009b; Yagura et al., 2015).

## 3. Results

### 3.1. Raltegravir single oral dose administration

The final PBPK model captured the concentration-time profiles observed in five clinical studies in healthy subjects in the fasted state (Figs. 2 and S4); 88.7% of the clinical data were within the simulated 5th–95th percentile range. Predicted/observed $AUC_{0-\infty}$, $T_{max}$, $C_{max}$, and CL/F parameter ratios in healthy volunteers are listed in Fig. 3. Eighteen out of twenty (90%) simulated PK parameters values were contained within a 2-fold error range.

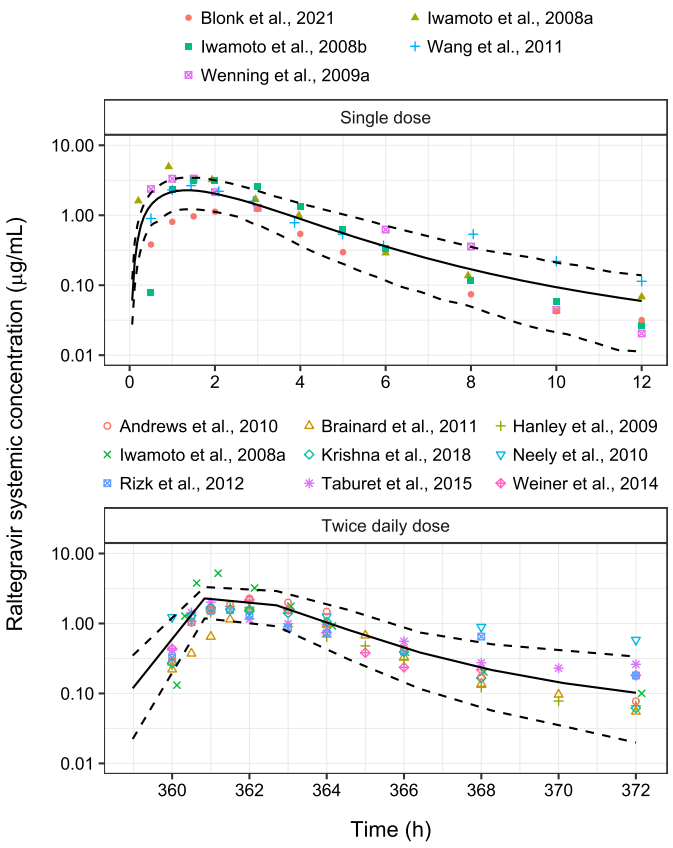


**Fig. 2.** Plot of the final PBPK raltegravir model. Plasma concentration-time profiles of raltegravir following a single oral dose of 400 mg or a twice-daily dose of 400 mg in the fasted state. The solid line represents the simulated mean plasma concentration, and the dotted lines represent simulated 5th and 95th percentiles.

### 3.2. Raltegravir multiple oral dosing regimen

Six clinical studies in healthy volunteers (Andrews et al., 2010; Hanley et al., 2009; Iwamoto et al., 2008a; Krishna et al., 2018; Neely et al., 2010; Weiner et al., 2014) and three clinical studies in HIV-infected patients (Brainard et al., 2011a; Rizk et al., 2012; Taburet et al., 2015) were evaluated regarding the raltegravir multiple oral dosing regimen. Predicted mean concentration-time profiles and associated 5th–95th prediction intervals of raltegravir after the 31$^{st}$ dose administration overlaid with the observed data, as shown in Figs. 2 and S5. More than 90% of the observed clinical concentration data were within the 5$^{th}$–95$^{th}$ percentile range. Predicted/observed ratios for the PK parameters $AUC_{0-12}$, $T_{max}$, trough plasma concentrations ($C_{trough}$), $C_{max}$, and CL/F in volunteers or patients treated with 400 mg twice daily oral dose raltegravir are listed in Fig. 3. Thirty-eight out of forty-five (84.4%) simulated PK parameters values were within a 2-fold error range.

### 3.3. Raltegravir UGT1A1 phenotypes

The verified PBPK models were applied to predict the effect of UGT1A1 phenotypes on raltegravir pharmacokinetics. After 400 mg raltegravir, as a single oral dose, the predicted means of concentration-time profiles and 5th–95th percentile range captured well the poor metabolizer phenotype (*28*28 genotype) when compared with the observed data (Fig. S6) (Belkhir et al., 2018).

The predicted/observed $C_{trough}$ values for UGT1A1 metabolizer phenotypes after 400 mg multiple doses are shown in Fig. 4. After 400 mg twice-daily oral doses of raltegravir, the predicted/observed $C_{trough}$

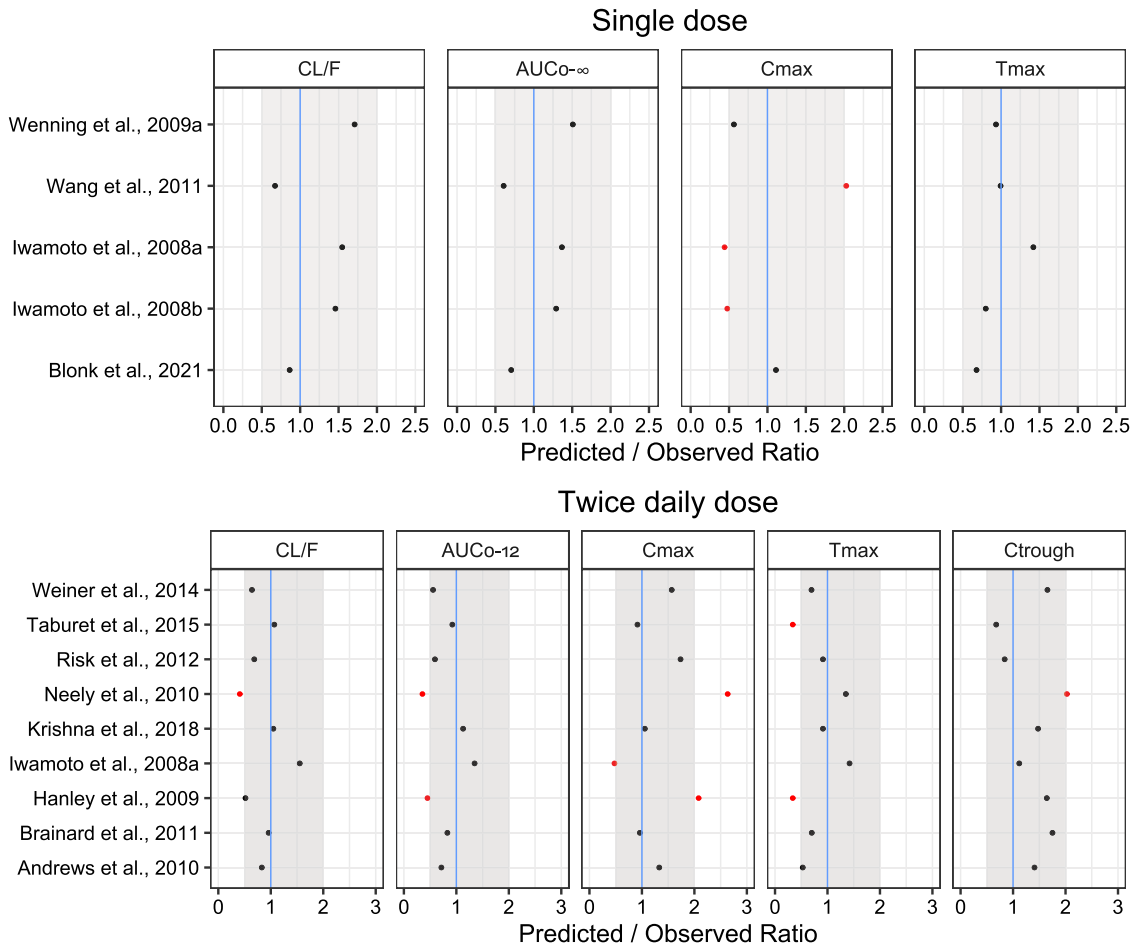


**Fig. 3.** Forest plot showing the raltegravir PBPK modeling performance. The solid line represents the identity (predicted/observed) ratio. The shaded area represents a 0.5 to 2-fold ratio window. The predicted/observed ratio in each clinical study is shown as dots.

ratio for the normal metabolizer phenotype were 0.86 and 1.10, considering two independent clinical trials (Belkhir et al., 2018; Yagura et al., 2015). The predicted/observed $C_{trough}$ ratio for intermediate metabolizer (*1*28 or *1*6 genotypes) was within a 2-fold error range (Moss et al., 2012; Sychterz et al., 2021). The $C_{trough}$ predicted/observed ratio for poor metabolizer was 0.67 relative to Belkhir et al. (2018) clinical study, which investigated UGT1A1*28 carriers, the most frequent variant allele in all populations. Nevertheless, predicted/observed $C_{trough}$ ratio for poor metabolizers were variable (0.11 to 0.41) and outside the 2-fold error range relative to Yagura et al. (2015) clinical study (*28*28; *6*28 and *6*6 genotypes). The more discrepant ratio was observed for the *6*6 genotype with a $C_{trough}$ predicted/observed ratio of 0.11-fold (Fig. 4). The high variability in the predictions for UGT1A1*6 carriers, which is relatively common in East Asian, but absent in Europan and African populations, is discussed below regarding the non-random association of UGT1A1 and 1A3 alleles.

## 4. Discussion

In the present study, a full PBPK model of raltegravir was developed and verified in healthy volunteers. The absorption model incorporates the intestinal permeability from *in vitro* Caco-2 cells experiments (Moss et al., 2011). Raltegravir is a class II drug according to the BDDCS classification, which suggests that gut and liver drug transporters might influence drug disposition (Benet et al., 2011). Class II drugs have low water solubility, high-fat solubility, and high permeability. Raltegravir (10 mM) was fully soluble at pH 6.8 or higher due to the deprotonation of the hydroxyl group (Moss et al., 2012). Increased raltegravir exposure is observed after high-fat food intake. High-fat meal resulted in a 2-fold increase in AUC and $C_{max}$ of raltegravir compared to fasted condition (Brainard et al., 2011b). Despite the increased plasma exposure, the magnitude of this food effect does not result in dosing recommendations for raltegravir when administered with specific meals (Isentress, 2008).

Raltegravir has shown pH-dependent dissolution with increasing oral bioavailability at higher pH values (Moss et al., 2013). The underprediction of $C_{max}$ observed in some simulated clinical studies can be attributed to the dynamic interplay of pH-dependent dissolution and drug transporters to the variability of raltegravir absorption (Komasaka et al., 2021). Raltegravir has been described as a substrate for the efflux transporters MDR1 P-gp and BCRP (Hoque et al., 2015), which are expressed in the apical membrane of the enterocytes (Hashiguchi et al., 2013; Hoque et al., 2015; Moss et al., 2011; Rizk et al., 2014; Zembruski et al., 2011). The efflux ratio obtained at the pH 6.5 in the apical compartment in Caco-2 cells was 1.6 (Moss et al., 2011), suggesting that active efflux is not the main contributor to raltegravir intestinal permeability. In fact, multiple doses of the P-glycoprotein inhibitor ritonavir did not change raltegravir AUC or $C_{max}$ (Hanley et al., 2009; Iwamoto et al., 2008b). Thus, P-glycoprotein was not incorporated in the final PBPK model, and the omitted mechanism is not expected to affect the predictions of raltegravir exposure.

For the full PBPK distribution model with 12 organs, both Poulin and Theil (method 1) and Rodgers and Rowland (methods 2 and 3) were tested. The Poulin and Theil equation described better raltegravir distribution, resulting in a Vss value of 0.34 l/kg with a tissue-plasma partition coefficient (Kp) scalar of 1. Other PBPK models used Poulin

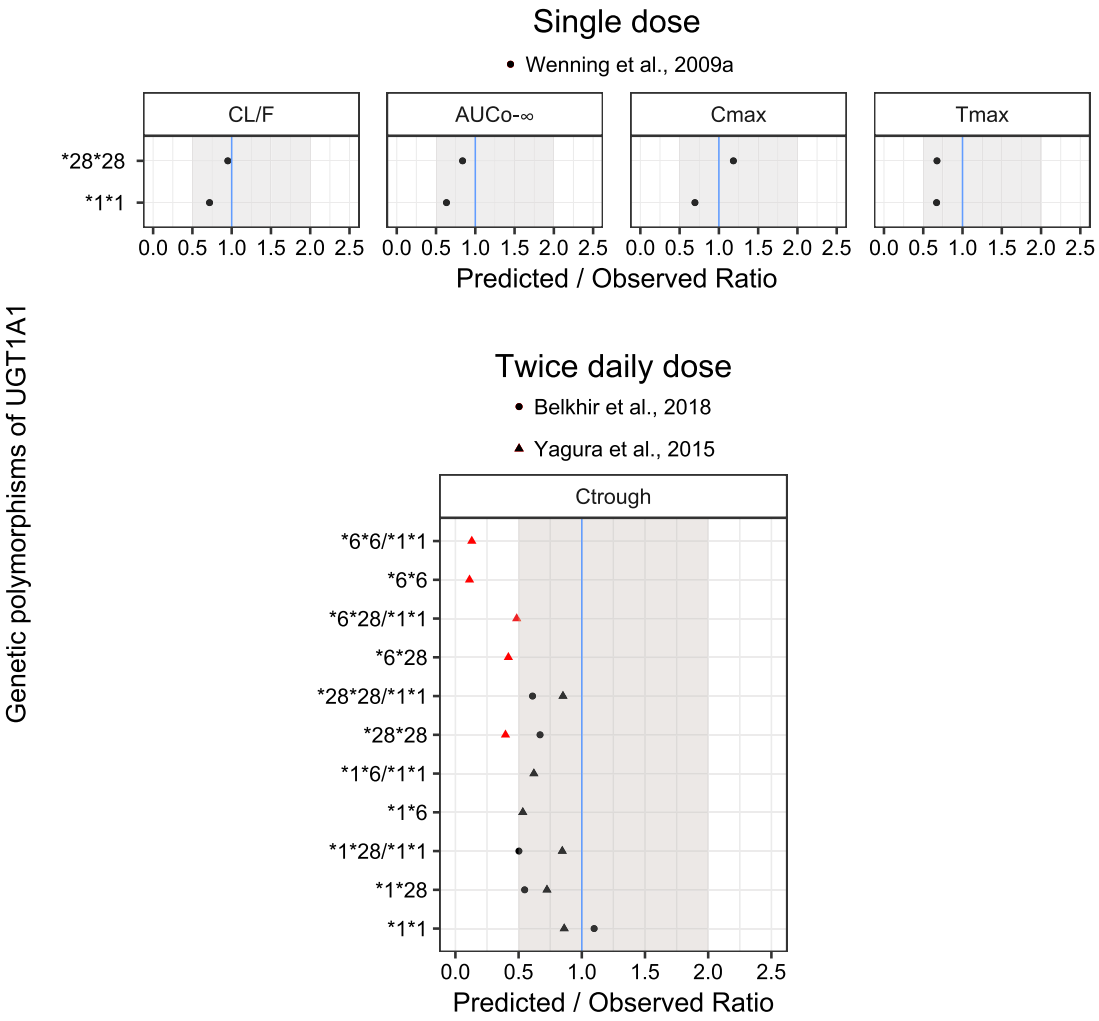


**Fig. 4.** Forest plot showing the PBPK modeling performance to assess the impact of UGT1A1 polymorphisms on raltegravir disposition. The solid line represents the identity (predicted/observed) ratio. The shaded area represents a 0.5 to 2-fold ratio window. Predicted/observed ratios in each clinical study are shown as dots or triangles.

and Theil equation to describe raltegravir distribution (Moss et al., 2013; Sychterz et al., 2021), except one using Rodgers and Rowland equation (Liu et al., 2020). The binding to cellular macromolecules, ionic interactions, and pH gradients within tissues are not accounted for by the Poulin and Theil model. Here, the homogenous tissue distribution by passive diffusion, described by Poulin and Theil method, captured raltegravir's Vss reasonably well (Obach et al., 2008).

The current raltegravir PBPK model accounts for hepatic, renal, and intestinal UGT1A1, 1A3, 1A7, 1A8, and 1A9-mediated metabolism, biliary clearance, and renal excretion. Glucuronidation of raltegravir is mediated by UGT enzymes. *In vitro* data using recombinant UGT isoforms have shown that UGT1A1 and UGT1A9 catalyzed raltegravir glucuronidation at similar rates, and UGT1A3, UGT1A7, and UGT1A8 showed lower rates (Liu et al., 2019). In contrast, Kassahun et al. (2007) demonstrated that the UGT1A1 glucuronidation rate was higher than that of UGT1A9 and UGT1A3. *In vitro in vivo* extrapolation with rhUGT/tissue scalar correction allowed to estimate the relative contribution of each UGT isoform in the liver, intestine, and kidney tissues *in vivo* (Reddy et al., 2021). Our PBPK approach has shown that the *in vivo* contribution of raltegravir metabolized by liver UGT1A3 (39.74%) was higher, followed by liver UGT1A9 (7.51%) and liver UGT1A1 (4.83%) (Fig. S7). It should be noted that UGT1A7 and UGT1A8 are not expressed in the liver (Kasteel et al., 2020). The model also accounted for the renal UGT isoforms with a relative contribution of 0.70%, 1.01%, 0.57%, and 0.49% of kidney UGT1A1, UGT1A9, UGT1A8, and UGT1A7 in raltegravir elimination, respectively.

Clinical studies have reported drug-drug interactions with raltegravir. Efavirenz, which modulates the expression of UGT enzymes by activating the pregnane X receptor, moderately reduces raltegravir AUC (Iwamoto et al., 2008a; Iwamoto et al., 2008b). Raltegravir exposure was slightly increased when combined with atazanavir, a known inhibitor of UGT1A1, UGT1A3, and UGT1A4 (Iwamoto et al., 2008a; Neely et al., 2010; Zhang et al., 2005; Zhu et al., 2010). In the absence of selective UGT isoforms inhibitors, the clinical DDI information is of limited value in assessing the contribution of UGT isoforms on raltegravir drug disposition. Leveraging *in vitro* metabolism data in recombinantly expressed systems (Liu et al., 2019), an extrapolation using UGT tissue scalars was performed to assess the contribution of UGT isoforms on raltegravir clearance. The inclusion of the additional mechanistic glucuronidation metabolism and appropriate physiological scalars and *in silico* modeling to accurately predict raltegravir elimination might be further used to explore other "*what if*" scenarios.

The PBPK model described by Liu et al. (2019) incorporated only *in vitro* data from UGT1A1 and UGT1A9 isoforms (Kassahun et al., 2007). The PBPK model developed by Sychterez (2021) used the optimized value of 1.48 μl/min/pmol for UGT1A1 intrinsic clearance, as in the default compound file provided by Simcyp software. Lastly, raltegravir elimination in the PBPK model proposed by Moss et al. (2013) was predicted using the intrinsic hepatic clearance fitted to clinical data. In the current work, the mechanistic model building based on recombinant

UGT isoforms data corrected by tissue scalar results in a promising predictive performance for future applications.

Some studies suggest the role of membrane transporters in raltegravir disposition. However, their relevance to the clinical context is still unknown. *In vitro* studies indicate that raltegravir is a substrate of human MDR1 (P-gp) and BCRP and renal uptake transporter OAT1. Still, it is not a substrate for OATP1B1, OATP1B3, OATP1A2, OCT1, sodium taurocholate cotransporting peptide (NTCP), and multidrug resistance proteins MRP1 (ABCC1), MRP2 (ABCC2), and MRP3 (ABCC3) (Hashiguchi et al., 2013; Hoque et al., 2015; Rizk et al., 2014). P-gp and BCRP are efflux drug transporters located in the biliary canaliculi of hepatocytes (Kock et al., 2012). The role of biliary excretion on raltegravir (fraction excreted of 15%) and raltegravir glucuronide (fraction excreted of 85%) disposition was previously described (Kassahun et al., 2007). From the underestimated raltegravir exposure in the multiple-dose during the PBPK model development (Fig. S8), the incorporation of biliary clearance and EHR was evaluated. The underestimation of raltegravir plasma exposure could be attributed to the saturation of metabolism processes. Nevertheless, non-linear pharmacokinetics was discarded since raltegravir AUC and $C_{max}$ are proportional up to 1600 mg doses (Isentress FDA, Drug Approval Package). Sensitivity analysis and parameter estimation were performed to obtain the biliary clearance value (12 μl/min/$10^{-6}$). The dose available for reabsorption in the gut was 100% in the final PBPK model. Secondary peaks are often observed in pharmacokinetic studies (Rizk et al., 2012; Taburet et al., 2015), and EHR is a reasonable explanation. The final model demonstrated an apparent fraction absorbed (relative to total oral dose) of 1.45, which is greater than unity, suggesting the relevance of EHR for raltegravir systemic exposure.

Raltegravir unchanged fraction eliminated in urine is reported to account for 2.9% (0.5–25.5%) after 400 mg single oral dose (Neely et al., 2010) or 9.95% and 11.4% after 400 mg single or twice-daily oral doses, respectively (Iwamoto et al., 2008b). The PBPK model developed in the current work is supported by data reported in clinical trials, as raltegravir unchanged fraction eliminated in urine was 11.1% after single or twice daily 400 mg raltegravir oral dose. The default raltegravir substrate file provided by Simcyp and employed by Sychterez (2021) results in 15.8% of renal contribution to overall raltegravir elimination. The current study and the PBPK model described by Sychterez (2021) used the renal clearance value of 3.3 L/h obtained from Neely et al., (2010), while the one reported by Moss et al. (2013) used the renal clearance value of 3.6 L/h obtained from Iwamoto et al. (2009). The PBPK model developed by Liu et al. (2020) reported the inclusion of renal elimination as the glomerular filtration rate fraction of 1. These data show that renal excretion is not a major route of elimination for raltegravir. Indeed, moderate or severe renal impairment is not clinically relevant to raltegravir drug disposition (Iwamoto et al., 2009).

The literature systematically describes UGT1A1 as the main raltegravir glucuronidation enzyme based on the *in vitro* assays performed by Kassahun et al. (2007). Consequently, the effect of UGT1A1 genetic polymorphisms on raltegravir pharmacokinetics was assessed in clinical trials. The microsatellite variation UGT1A1*28, including an extra TATA box sequence A(TA)$_7$TAA, slightly decreased the glucuronidation activity and increased raltegravir AUC values for raltegravir (Wenning et al., 2009b; Yagura et al., 2015; Belkhir et al., 2018). The single nucleotide polymorphism *UGT1A1* c.211G>A (UGT1A1*6), which is rare in Caucasian and African Americans but common in Asian populations, was associated with higher plasma concentrations of raltegravir (Yagura et al., 2015). The PBPK model described by Sychterez et al. (2021), which did not account for UGT1A3, 1A7, 1A8, or 1A9, overpredicted the increased raltegravir plasma exposure in UGT1A1 poor metabolizers. Our findings suggest that UGT1A3 activity is the main contributor to raltegravir elimination. Accordingly, UGT1A3 pharmacogenetics showed a higher impact than UGT1A1 on raltegravir kinetic disposition (Fig. 5). Here, the predicted/observed ratios were lower than unity in *UGT1A1* poor metabolizers. This behavior was evident for simulations compared to the *UGT1A1* *6/*6 diplotype, which are mainly found in the Asian population. A reasonable explanation is the linkage disequilibrium (LD) between UGT1A1 and 1A3 variants described in Japanese. *UGT1A1*6 and *UGT1A3*4a have shown significant disequilibrium (D' = 1) (Ieiri et al., 2011). The amino acid change R45W in *UGT1A3*4a was previously associated with 70% of enzyme activity, evaluated as estrone glucuronidation rate relative to the wild type (Iwai et al., 2004). As the UGT1A3 poor metabolizer (PM) phenotype was not assessed in clinical trials and not incorporated into the model concomitant to the UGT1A1 PM phenotype, the current model underpredicts the combined effect of *UGT1A3* and *UGT1A1* gene polymorphisms, which is expected in Asian *UGT1A1*6 carriers. Supposing that our hypothesis on the interplay of UGT1A1 × UGT1A3 gene polymorphisms confirms in the clinics, increased plasma exposure to raltegravir may be observed in UGT1A3 PM/UGT1A1 PM subjects. Our simulations have shown that UGT1A3 PM/UGT1A1 PM subjects show a 2.7-fold increase in raltegravir AUC compared to UGT1A3/UGT1A1 normal metabolizers (NM). Since raltegravir is considered a safe drug even at high doses, dose adjustments in UGT1A3 NM/UGT1A1 NM may be recommended to avoid drug wastage.

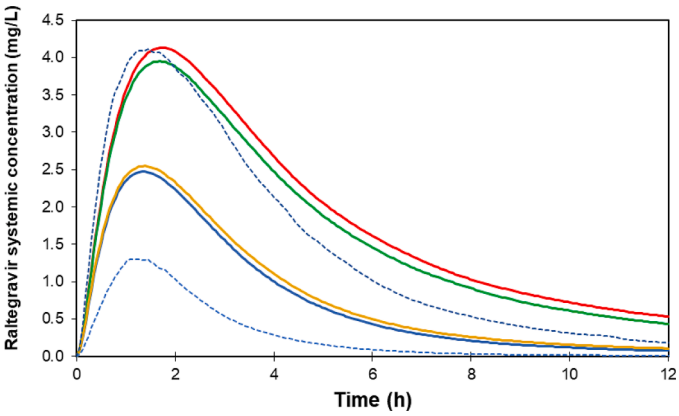


**Fig. 5.** PK profiles in different UGT1A1 and UGT1A3 metabolizer phenotypes. NM: normal metabolizer; PM: poor metabolizer. Simulation on UGT1A1 NM/UGT1A3 NM was set as a reference (mean predictions in solid blue line and 5th-95th percentiles of predictions in dashed blue lines). UGT1A1 PM/UGT1A3 NM, UGT1A1 NM/UGT1A3 PM and UGT1A1 PM/UGT1A3 PM: are displayed in yellow, green and red, respectively.

In conclusion, our findings suggest that UGT1A3 activity is the main contributor to raltegravir elimination. As the effect of UGT1A3 pharmacogenetics was not previously assessed in clinical trials, our simulations anticipate that UGT1A3 has a higher impact than UGT1A1 on raltegravir kinetic disposition (Fig. 5). Other gene polymorphisms in LD between UGT1A1 and 1A3 variants cannot be discarded, and the interplay of genetic polymorphisms of UGT1A1 and 1A3 in raltegravir metabolism needs to be investigated in clinical trials. The current PBPK model for raltegravir has some limitations. The lack of a permeability-limited model considering the main drug transporters involved in raltegravir disposition limits the evaluation of drug-drug interaction or drug-disease interactions related to transporters. The addition of mechanistic *in vitro* data of drug transporters expressed in key tissues for raltegravir disposition could significantly increase the predictive capacity of this model. All simulations were performed using the virtual library populations of healthy volunteers. HIV-AIDS patients can present disturbances in the GI tract such as elevated gastric pH, decreased gastric transit time, decreased intestinal absorption surface area, diarrhea, and fat malabsorption syndromes (for lipid-soluble drugs) (Hatton et al., 2019). These factors can affect raltegravir bioavailability. So, building an HIV-infected population could improve the predictions for the raltegravir concentration-time profiles in this population.

## 5. Conclusions

The developed PBPK model successfully predicted the mean raltegravir PK profile after 400 mg single and multiple oral doses and might be applied to different clinical scenarios. Overall, the PBPK model adequately predicted the pharmacokinetic changes associated with UGT1A1 genotype/phenotype, except for UGT1A1*6 carriers. The *in vitro in vivo* extrapolation proposed here suggests that UGT1A3 is the main contributor to raltegravir metabolism. UGT1A3 and UGT1A1 genetic polymorphisms might have an additive effect on raltegravir drug disposition and response. The current approach improved the predictive performance compared with the previously published raltegravir models. The final model accounts for liver, kidney, and intestine UGT metabolism, biliary clearance, and renal excretion. Due to the robust characterization of elimination pathways, this PBPK model can support raltegravir dose adjustments in different clinical scenarios.

## Data availability

The authors can share the input parameters upon request.

## CRediT authorship contribution statement

**Fernanda-de-Lima Moreira:** Conceptualization, Methodology, Writing – original draft, Writing – review & editing, Visualization, Investigation, Formal analysis. **Maria-Martha-de-Barros Tarozzo:** Methodology, Investigation, Writing – review & editing. **Glauco-Henrique-Balthazar Nardotto:** Formal analysis, Writing – review & editing. **José-Carlos-Saraiva Gonçalves:** Writing – review & editing, Formal analysis, Writing – review & editing. **Stephan Schmidt:** Writing – review & editing, Formal analysis, Writing – review & editing. **Natália-Valadares de-Moraes:** Methodology, Writing – review & editing, Formal analysis, Writing – review & editing.

## Declaration of Competing Interest

The authors declare no conflict of interest

## Funding information

No funding was received for this work

## Supplementary materials

Supplementary material associated with this article can be found, in the online version, at doi:10.1016/j.ejps.2022.106309.

## References

Andrews, E., Glue, P., Fang, J., Crownover, P., Tressler, R., Damle, B., 2010. Assessment of the pharmacokinetics of co-administered maraviroc and raltegravir. Br. J. Clin. Pharmacol. 69, 51–57.

Belkhir, L., Seguin-Devaux, C., Elens, L., Pauly, C., Gengler, N., Schneider, S., Ruelle, J., Haufroid, V., Vandercam, B., 2018. Impact of UGT1A1 polymorphisms on raltegravir and its glucuronide plasma concentrations in a cohort of HIV-1 infected patients. Sci. Rep. 8, 7359.

Benet, L.Z., Broccatelli, F., Oprea, T.I., 2011. BDDCS applied to over 900 drugs. AAPS J. 13, 519–547.

Blonk, M., Colbers, A., Poirters, A., Schouwenberg, B., Burger, D., 2012. Effect of ginkgo biloba on the pharmacokinetics of raltegravir in healthy volunteers. Antimicrob. Agents Chemother. 56, 5070–5075.

Blonk, M.I., Colbers, A.P., Hidalgo-Tenorio, C., Kabeya, K., Weizsäcker, K., Haberl, A.E., Moltó, J., Hawkins, D.A., van der Ende, M.E., Gingelmaier, A., Taylor, G.P., Ivanovic, J., Giaquinto, C., Burger, D.M., 2015. Pharmacokinetics of newly developed antiretroviral agents in HIV-infected pregnant women PANNA Network; PANNA network. Raltegravir in HIV-1-infected pregnant women: pharmacokinetics, safety, and efficacy. Clin. Infect. Dis. 61, 809–816.

Brainard, DM, Friedman, EJ, Jin, B, et al., 2011b. Effect of low-, moderate-, and high-fat meals on raltegravir pharmacokinetics. J. Clin. Pharmacol. 51 (3), 422–427.

Brainard, D.M., Kassahun, K., Wenning, L.A., Petry, A.S., Liu, C., Lunceford, J., Hariparsad, N., Eisenhandler, R., Norcross, A., DeNoia, E.P., Stone, J.A., Wagner, J. A., Iwamoto, M., 2011a. Lack of a clinically meaningful pharmacokinetic effect of rifabutin on raltegravir: *in vitro/in vivo* correlation. J. Pharmacol. 51, 943–950.

Cattaneo, D., Gervasoni, C., Meraviglia, P., Landonio, S., Fucile, S., Cozzi, V., Baldelli, S., Pellegrini, M., Galli, M., Clementi, E., 2012. Inter- and intra-patient variability of raltegravir pharmacokinetics in HIV-1-infected subjects. J. Antimicrob. Chemother. 67, 460–464.

Gammal, R.S., Court, M.H., Haidar, C.E., Iwuchukwu, O.F., Gaur, A.H., Alvarellos, M., Guillemette, C., Lennox, J.L., Whirl-Carrillo, M., Brummel, S.S., Ratain, M.J., Klein, T.E., Schackman, B.R., Caudle, K.E., Haas, D.W., 2016. Clinical pharmacogenetics implementation consortium (CPIC) guideline for UGT1A1 and atazanavir prescribing. Clin. Pharmacol. Therap. 99, 363–369.

Hanley, W.D., Wenning, L.A., Moreau, A., Kost, J.T., Mangin, E., Shamp, T., Stone, J.A., Gottesdiener, K.M., Wagner, J.A., Iwamoto, M., 2009. Effect of tipranavir-ritonavir on pharmacokinetics of raltegravir. Antimicrob. Agents Chemother. 53, 2752–2755.

Hashiguchi, Y., Hamada, A., Shinohara, T., Tsuchiya, K., Jono, H., Saito, H., 2013. Role of P-glycoprotein in the efflux of raltegravir from human intestinal cells and CD4+ T-cells as an interaction target for anti-HIV agents. Biochem. Biophys. Res. Commun. 439, 221–227.

Hatton, G.B., Madla, C.M., Rabbie, SC, Basit, AW, 2019. Gut reaction: impact of systemic diseases on gastrointestinal physiology and drug absorption. Drug Discov. Today 24, 417–42743.

Hoque, M.T., Kis, O., De Rosa, M.F., Bendayan, R., 2015. Raltegravir permeability across blood-tissue barriers and the potential role of drug efflux transporters. Antimicrob. Agents Chemother. 59, 2572–2582.

Ieiri, I., Nishimura, C., Maeda, K., Sasaki, T., Kimura, M., Chiyoda, T., Hirota, T., Irie, S., Shimizu, H., Noguchi, T., Yoshida, K., Sugiyama, Y., 2011. Pharmacokinetic and pharmacogenomic profiles of telmisartan after the oral microdose and therapeutic dose. Pharmacogenet Genom. 21, 495–505.

Isentress, 2008. FDA Drug approval package. https://www.accessdata.fda.gov/drugsatfda_docs/nda/2007/022145_ (acessed June 15 2022).

European Medicines Agency, 2015. Guideline on the investigation of drug interactions. https://www.ema.europa.eu/en/documents/scientific-guideline/guideline-investigation-drug-interactions-revision-1_en.pdf (accessed June 13 2022).

Iwai, M., Maruo, Y., Ito, M., Yamamoto, K., Sato, H., Takeuchi, Y., 2004. Six novel UDP-glucuronosyltransferase (UGT1A3) polymorphisms with varying activity. J. Hum. Genet. 49, 123–128.

Iwamoto, M., Wenning, L.A., Petry, A.S., Laethem, M., De Smet, M., Kost, J.T., Breidinger, S.A., Mangin, E.C., Azrolan, N., Greenberg, H.E., Haazen, W., Stone, J.A., Gottesdiener, K.M., Wagner, J.A., 2008a. Minimal effects of ritonavir and efavirenz on the pharmacokinetics of raltegravir. Antimicrob. Agents Chemother. 52, 4338–4343.

Iwamoto, M., Wenning, L.A., Petry, A.S., Laethem, M., De Smet, M., Kost, J.T., Merschman, S.A., Strohmaier, K.M., Ramael, S., Lasseter, K.C., Stone, J.A., Gottesdiener, K.M., Wagner, J.A., 2008b. Safety, tolerability, and pharmacokinetics of raltegravir after single and multiple doses in healthy subjects. Clin. Pharmacol. Ther. 83, 293. -239.

Iwamoto, M., Hanley, W.D., Petry, A.S., Friedman, E.J., Kost, J.T., Breidinger, S.A., Lasseter, K.C., Robson, R., Lunde, N.M., Wenning, L.A., Stone, J.A., Wagner, J.A., 2009. Lack of a clinically important effect of moderate hepatic insufficiency and severe renal insufficiency on raltegravir pharmacokinetics. Antimicrob. Agents Chemother. 53, 1747–1752.

Jones, H., Rowland-Yeo, K., 2013. Basic concepts in physiologically based pharmacokinetic modeling in drug discovery and development. CPT Pharmacomet. Syst. Pharmacol. 2, e63.

Kassahun, K., McIntosh, I., Cui, D., Hreniuk, D., Merschman, S., Lasseter, K., Azrolan, N., Iwamoto, M., Wagner, J.A., Wenning, L.A., 2007. Metabolism and disposition in humans of raltegravir (MK-0518), an Anti-AIDS Drug targeting the human immunodeficiency virus 1 integrase enzyme. Drug Metab. Dispos. 35, 1657–1663.

Kasteel, E.E.J., Darney, K., Kramer, N.I., Dorne, J.L.C.M., Lautz, L.S., 2020. Human variability in isoform-specific UDP-glucuronosyltransferases: markers of acute and chronic exposure, polymorphisms and uncertainty factors. Arch. Toxicol. 94, 2637–2661.

Kock, K., Brouwer, K.L.R., 2012. A Perspective on efflux transport proteins in the liver. Clin. Pharmacol. Therap. 92, 599–612.

Komasaka, T., Dressman, J., 2021. Simulation of oral absorption from non-bioequivalent dosage forms of the salt of raltegravir, a poorly soluble acidic drug, using a physiologically based biopharmaceutical modeling (PBBM) approach. Eur. J. Pharm. Sci. 157, 105630.

Krishna, R., Rizk, M.L., Larson, P., Schulz, V., Kesisoglou, F., Pop, R., 2018. Single- and multiple-dose pharmacokinetics of once-daily formulations of raltegravir. Clin. Pharmacol. Drug Dev. 7, 196–206.

Ladumor, MK, Thakur, A, Sharma, S, Rachapally, A., Mishra, S., Bobe, P., Rao, V.K., Pammi, P., Kangne, H., Levi, D., Balhara, A., Ghandikota, S., Joshi, A., Nautiyal, V., Prasad, B., Singh, S., 2019. A repository of protein abundance data of drug metabolizing enzymes and transporters for applications in physiologically based pharmacokinetic (PBPK) modelling and simulation. Sci. Rep. 9, 9709.

Liu, S.N., Lu, J.B.L., Watson, C.J.W., Lazarus, P., Desta, Z., Gufford, B.T., 2019. Mechanistic assessment of extrahepatic contributions to glucuronidation of integrase strand transfer inhibitors. Drug Metab. Dispos. 47, 535–544.

Liu, X.I., Momper, J.D., Rakhmanina, N.Y., Green, D.J., Burckart, G.J., Cressey, T.R., Mirochnick, M., Best, B.M., van den Anker, J.N., Dallmann, A., 2020. Prediction of maternal and fetal pharmacokinetics of dolutegravir and raltegravir using physiologically based pharmacokinetic modeling. Clin. Pharmacokinet. 59, 1433–5140.

Moss, D.M., Kwan, W.S., Liptrott, N.J., Smith, D.L., Siccardi, M., Khoo, S.H., Back, D.J., Owen, A., 2011. Raltegravir is a substrate for SLC22A6: a putative mechanism for the

interaction between raltegravir and tenofovir. Antimicrob. Agents Chemother. 55, 879–887.
Moss, D.M., Siccardi, M., Back, D.J., Owen, A., 2013. Predicting intestinal absorption of raltegravir using a population-based ADME simulation. J. Antimicrob. Chemother. 68, 1627–1634.
Moss, D.M., Siccardi, M., Murphy, M., Piperakis, M.M., Khoo, S.H., Back, D.J., Owen, A., 2012. Divalent metals and pH alter raltegravir disposition *in vitro*. Antimicrob. Agents Chemother. 56, 3020–3026.
Neely, M., Decosterd, L., Fayet, A., Lee, J.S., Margol, A., Kanani, M., di Iulio, J., von Schoen-Angerer, T., Jelliffe, R., Calmy, A., 2010. Pharmacokinetics and pharmacogenomics of once-daily raltegravir and atazanavir in healthy volunteers. Antimicrob. Agents Chemother. 54, 4619–4625.
Obach, R.S., Lombardo, F., Waters, N.G., 2008. Trend analysis of a database of intravenous pharmacokinetic parameters in humans for 670 drug compounds. Drug Metab. Dispos. 36, 1385–1405.
Peters, S.A., Dolgos, H., 2019. Requirements to establishing confidence in physiologically based pharmacokinetic (PBPK) models and overcoming some of the challenges to meeting them. Clin. Pharmacokinet. 58, 1355–1371.
Reddy, M.B., Bolger, M.B., Fraczkiewicz, G., Del Frari, L., Luo, L., Lukacova, V., Mitra, A., Macwan, J.S., Mullin, J.M., Parrott, N., Heikkinen, A.T., 2021. PBPK modeling as a tool for predicting and understanding intestinal metabolism of uridine 5'-diphospho-glucuronosyltransferase substrates. Pharmaceutics 13, 1325.
Rizk, M.L., Hang, Y., Luo, W.L., Su, J., Zhao, J., Campbell, H., Nguyen, B.Y., Sklar, P., Eron Jr., J.J., Wenning, L., 2012. Pharmacokinetics and pharmacodynamics of once-daily versus twice-daily raltegravir in treatment-naïve HIV-infected patients. Antimicrob. Agents Chemother. 56, 3101–3106.
Rizk, M.L., Houle, R., Chan, G.H., Hafey, M., Rhee, E.G., Chu, X., 2014. Raltegravir has a low propensity to cause clinical drug interactions through inhibition of major drug transporters: an *in vitro* evaluation. Antimicrob. Agents Chemother. 58, 1294–1301.
Sychterz, C., Galetin, A., Taskar, K.S., 2021. When special populations intersect with drug–drug interactions: application of physiologically-based pharmacokinetic modeling in pregnant populations. Biopharm. Drug Dispos. 42, 160–177.
Taburet, A.M., Sauvageon, H., Grinsztejn, B., Assuied, A., Veloso, V., Pilotto, J.H., De Castro, N., Grondin, C., Fagard, C., Molina, J.M., 2015. Pharmacokinetics of raltegravir in HIV-infected patients on rifampicin-based antitubercular therapy. HIV/AIDS 61, 1328–1335.
Wang, L., Soon, G.H., Seng, K.Y., Li, J., Lee, E., Yong, E.L., Goh, B.C., Flexner, C., Lee, L., 2011. Pharmacokinetic modeling of plasma and intracellular concentrations of raltegravir in healthy volunteers. Antimicrob. Agents Chemother. 55, 4090–4095.
Watts, D.H., Stek, A., Best, B.M., Wang, J., Capparelli, E.V., Cressey, T.R., Aweeka, F., Lizak, P., Kreitchmann, R., Burchett, S.K., Shapiro, D.E., Hawkins, E., Smith, E., Mirochnick, M., IMPAACT 1026s study team, 2014. Raltegravir pharmacokinetics during pregnancy. J. Acquir. Immune Defic. Syndr. 67, 375–381.
Weiner, M., Egelund, E.F., Engle, M., Kiser, M., Prihoda, T.J., Gelfond, J.A., Mac Kenzie, W., Peloquin, C.A., 2014. Pharmacokinetic interaction of rifapentine and raltegravir in healthy volunteers. J. Antimicrob. Chemother. 69, 1079–1085.
Wenning, L.A., Hanley, W.D., Brainard, D.M., Petry, A.S., Ghosh, K., Jin, B., Mangin, E., Marbury, T.C., Berg, J.K., Chodakewitz, J.A., Stone, J.A., Gottesdiener, K.M., Wagner, J.A., Iwamoto, M., 2009a. Effect of rifampin, a potent inducer of drug-metabolizing enzymes, on the pharmacokinetics of raltegravir. Antimicrob. Agents Chemother. 53, 2852–2856.
Wenning, L.A., Petry, A.S., Kost, J.T., Jin, B., Breidinger, S.A., DeLepeleire, I., Carlini, E. J., Young, S., Rushmore, T., Wagner, F., Lunde, N.M., Bieberdorf, F., Greenberg, H., Stone, J.A., Wagner, J.A., Iwamoto, M., 2009b. Pharmacokinetics of raltegravir in individuals with UGT1A1 polymorphisms. Clin. Pharmacol. Therap. 85, 623–627.
Yagura, H., Watanabe, D., Ashida, M., Kushida, H., Hirota, K., Ikuma, M., Ogawa, Y., Yajima, K., Kasai, D., Nishida, Y., Uehira, T., Yoshino, M., Shirasaka, T., 2015. Correlation between UGT1A1 polymorphisms and raltegravir plasma trough concentrations in Japanese HIV-1-infected patients. J. Infect. Chemother. 21, 713–717.
Zembruski, N.C., Büchel, G., Jödicke, L., Herzog, M., Haefeli, W.E., Weiss, J., 2011. Potential of novel antiretrovirals to modulate expression and function of drug transporters *in vitro*. J. Antimicrob. Chemother. 66, 802–812.
Zhang, D., Chando, T.J., Everett, D.W., Patten, C.J., Dehal, S.S., Humphreys, W.G., 2005. *In vitro* inhibition of UDP glucuronosyltransferases by atazanavir and other HIV protease inhibitors and the relationship of this property to *in vivo* bilirubin glucuronidation. Drug Metab. Dispos. 33, 1729. -1139.
Zhu, L., Butterton, J., Persson, A., Stonier, M., Comisar, W., Panebianco, D., Breidinger, S., Zhang, J., Bertz, R., 2010. Pharmacokinetics and safety of twice-daily atazanavir 300 mg and raltegravir 400 mg in healthy individuals. Antivir. Ther. 15, 1107–1114.